A MODERN ANSWER IN MATTER OF PRECISION TRACKING : STEPWISE RAY-TRACING

F. Méot (CEA DAPNIA, Saclay) and **F. Lemuet** (CERN AB/ABP)

CARE/HHH workshop, CERN, Nov. 2004.

Abstract

Precision tracking is not only a matter of integrator simplecticity, it also requires accuracy in modelling of magnetic fields, their non-linearities and possible defects. Stepwise ray-tracing can make the best use of these two crucial prerequisites regarding precision integration ; allied with the computing speed of modern computers, this results in high performance tools. The topic is discussed through recent developments in the ray-tracing code Zgoubi, aimed at multiturn tracking in the strongly non-linear fields of fixed field alternating gradient synchrotrons.

INTRODUCTION

From the early years of synchrotron developments, stepwise ray-tracing has been considered a good technique to integrate particle motion, allowing the drawing of machine parameters from single- or multi-turn tracking, possibly using magnet field maps [1]. The developments presented here are based on such methods using the ray-tracing code Zgoubi [2].

Zgoubi has long been used in synchrotron studies (*cf.*, LHC [3], FNAL recycler ring [4], muon storage rings [5]), and the recent developments in the code discussed here further permit the difficult simulation of large amplitude, multi-turn 6-D tracking in scaling and non-scaling FFAGs, for which only a few codes have been applied [6].

Ray-tracing thus offers a mean for fast optimization of FFAG magnet geometry and fields as constrained by design parameters ; it provides correct simulation of multiturn motion, with such outcomes as the right computation of lattice tunes, tune variations, time of flight, etc. ; it yields precision 6-D multiturn tracking and motion stability limits in FFAGs.

In the following, the methods for simulating FFAG fields are described, and then applied to various problems of 6-D or 4-D tracking in FFAG rings, scaling and isochronous.

RAY-TRACING METHOD, INGREDIENTS

We first recall the ingredients of the Zgoubi method that intervene in the implementation of dipole N-uplet simulations.

Position and velocity The integration method is based on stepwise resolution of Lorentz equation by a technique of Taylor series. The working frame is shown in Fig. 1. Position and velocity of a particle subject to $m d\vec{v}/dt = q\,\vec{v}\times\vec{b}$ are tracked using truncated Taylor expansions in the integration step Δs

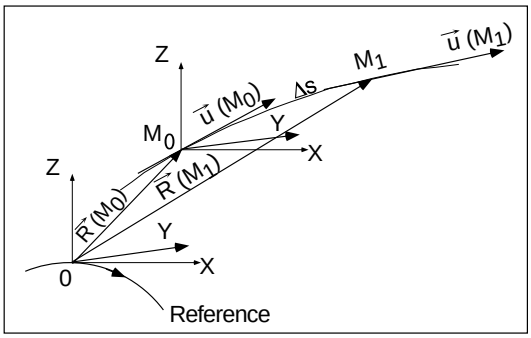

Figure 1: Zgoubi frame and coordinates.

$$\begin{aligned}\vec{R}(M_1) &\approx \vec{R}(M_0) + \vec{u}(M_0)\,\Delta s + \vec{u}'(M_0)\,\tfrac{\Delta s^2}{2!} + ... \quad (1)\\ \vec{u}(M_1) &\approx \vec{u}(M_0) + \vec{u}'(M_0)\,\Delta s + \vec{u}''(M_0)\,\tfrac{\Delta s^2}{2!} + ...\end{aligned}$$

wherein $\vec{u} = \vec{v}/v$, $\Delta s = v\,\Delta t$, $\vec{u}' = d\vec{u}/ds$, $m\vec{v} = mv\vec{u} = q\,B\rho\,\vec{u}$, and with the derivatives $\vec{u}^{(n)} = d^n\vec{u}/ds^n$ given by $\vec{u}' = \vec{u}\times\vec{B}$, $\vec{u}'' = \vec{u}'\times\vec{B} + \vec{u}\times\vec{B}'$, $\vec{u}''' = \vec{u}''\times\vec{B} + 2\vec{u}'\times\vec{B}' + \vec{u}\times\vec{B}''$, etc.

Taylor coefficients Computation of the coefficients in Eqs. 1 requires the knowledge of the magnetic field $\vec{B}(s)$ and derivatives $d^n\vec{B}/ds^n \quad (n \le 5)$ in the orthogonal frame (O,X,Y,Z) (Fig. 1). On the other hand, the magnetic field in a dipole can be obtained from a mid-plane model of the vertical field component (the horizontal component is zero by symmetry), in cylindrical coordinates, of the form $B_z(r,\theta) = B_{z0}\,\mathcal{F}(r,\theta)\,\mathcal{R}(r)$, with factors $\mathcal{F}(r,\theta)$ and $\mathcal{R}(r)$ accounting for the longitudinal (e.g., field fall-offs at dipoles' ends) and for the transverse (e.g., transverse non-linearities) variation of the dipole field. The way the mid-plane field and its derivatives $B_z(r,\theta), \quad \frac{\partial^{k+l}B_z}{\partial\theta^k\partial r^l}$ at all (r,θ) are obtained from this model is detailed below.

Once this is done, a transformation from the cylindrical frame of the magnet into the Cartesian frame in Fig. 1 is performed, next, Z-derivatives and extrapolation off mid-plane are obtained from Maxwell equations and Taylor expansions, thus yielding the 3-D field description

$$\vec{B}(X,Y,Z), \qquad \frac{\partial^{k+l+m}\vec{B}}{\partial X^k\partial Y^l\partial Z^m}$$

Eventually, $\vec{B}(s)$ and $d^n\vec{B}/ds^n$ needed in Eqs. 1 are derived by appropriate coordinate transformations.

STRONGLY NON-LINEAR FIELDS

Two new procedures, named "`DIPOLES`" and "`FFAG`", have been installed in the ray-tracing code for the purposes

outlined [7]. They can account for overlapping fields in the case of neighboring dipoles (Figs. 2-a,b). Dipoles are defined by their parameters as wedge angles, pole curvature, fringe field extents, etc., [2, b], and are positioned within a sector region with angle AT, by means of angles ACN_i. The (r, θ) field dependence has the form

$$B_{zi}(r,\theta) = B_{z0,i}\,\mathcal{R}_i(r)\,\mathcal{F}_i(r,\theta) \qquad (2)$$

(the index i stands for the dipole of concern in an N-uplet). "DIPOLES" and "FFAG" differ by the radial behavior, respectively

$$\mathcal{R}_i(r) = b_{0_i} + b_{1_i}\frac{r-R_{0,i}}{R_{0,i}} + b_{2_i}\left(\frac{r-R_{0,i}}{R_{0,i}}\right)^2 + ..., \qquad (3)$$

$$\mathcal{R}_i(r) = (r/R_{0,i})^{K_i} \qquad (4)$$

The first form of $\mathcal{R}_i(r)$ is proper to simulate FFAG

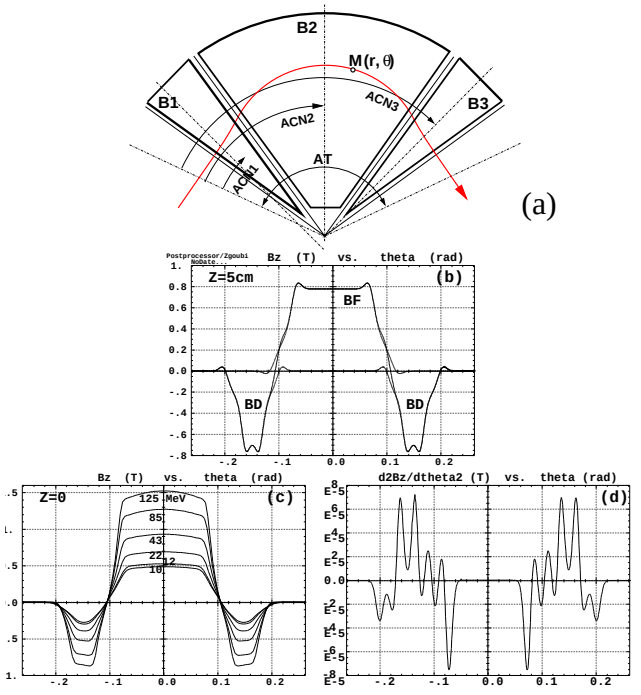

Figure 2: (a) : FFAG sector triplet. (b) : example of overlapping fields at constant radius, the three field contributions are represented separately, together with their merging. (c) : mid-plane field on closed orbits at various energies. (d) : a sample field derivative on closed orbit, $\partial^2 B_z(r,\theta)/\partial\theta^2$.

isochronous lattices [8], SC magnets [9], non-scaling FFAG lattices [10], etc., by *ad hoc* values of the b_{j_i} coefficients. The second form is specific to scaling FFAG. The axial dependence $\mathcal{F}_i(r,\theta)$ is modeled using fall-offs at *EFBs* of the form

$$\mathcal{F}_{EFB}(d) = (1+\exp[P(d)])^{-1}$$

with $P(d) = C_0 + C_1 d/g + C_2(d/g)^2 + \ ... \ + C_5(d/g)^5$

wherein d is the distance to the *EFB* and depends on r and θ ; the normalizing coefficient g is in general of the form

$$g(r) = g_0(R_0/r)^\kappa$$

($\kappa \geq 0$) with g_0 the dipole gap. A dipole having two *EFBs* (entrance and exit) with each one its own fringe field factor, the resulting form factor at (r,θ) due to dipole (i) of the N-uplet is thus taken to be

$$\mathcal{F}_i(r,\theta) = \mathcal{F}_{\text{Entrance}}(r,\theta) \times \mathcal{F}_{\text{Exit}}(r,\theta)$$

The total mid-plane field and derivatives at (r,θ) in an N-uplet are obtained by summing the contributions of the N dipoles taken separately (*e.g.*, $N=3$ in Fig. 2), namely

$$B_z(r,\theta) = \sum_{i=1,N} B_{z0,i}\,\mathcal{R}_i(r)\,\mathcal{F}_i(r,\theta)\,,$$

$$\frac{\partial^{k+l}\vec{B}_z(r,\theta)}{\partial r^k \partial\theta^l} = \sum_{i=1,N}\frac{\partial^{k+l}\vec{B}_{zi}(r,\theta)}{\partial r^k\partial\theta^l} \qquad (5)$$

Eventually, the 6-D field model $\vec{B}(r,\theta,z)$ and derivatives $\partial^{k+l+m}\vec{B}/\partial r^k\partial\theta^l\partial z^m$ are deduced by z-extrapolation. Sample $B_z(r,\theta)$ patterns, using the scaling field model in Eq. 4, are given in Figs. 2-b-c, a simulation of the field in an FFAG triplet with characteristics drawn from the KEK 150 MeV proton machine [11].

6-D TRACKING IN A SCALING FFAG

We now show that these methods provide correct results, by applying it to 6-D tracking in a scaling FFAG ring.

A 12-cell scaling FFAG ring is considered, representative of the KEK 150 MeV proton FFAG [11]. The cell is a 30 degree sector encompassing a DFD triplet, with $K = 7.6$ in Eq. 4, yielding field on closed orbits as schemed in Figs. 2-b-c, and quasi-zero chromaticity in both planes. Closed orbits in a cell and one-turn tunes are displayed in Fig. 3 ; with optimized integration step size, tunes values can be guaranteed with good accuracy, better than 10^{-4}. Other first order results, as drawn from multiturn tracking, are displayed in Tab. 1 and show satisfying consistency with published data [11, 12], the momentum compaction satisfies $\alpha \approx 1/(1+K)$. The vertical chromaticity is not exactly zero due to the fringe fields (zero vertical chromaticity is obtained as expected when a geometrical model with hard edge is used [7]). Fig. 4 shows sample phase space motion at 50 MeV. The horizontal symplecticity is very good. The vertical motion shows confined emittance spread, attributed to non-linear coupling.

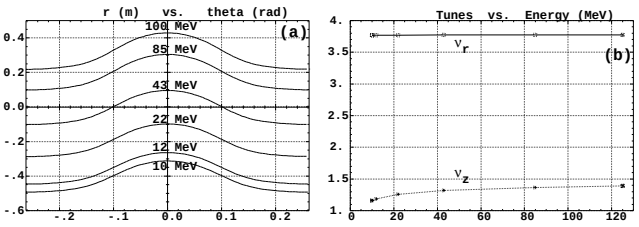

Figure 3: (a) : closed orbits in a cell. (b) : one-turn tunes.

Next, stationary bucket dynamics has been simulated (Fig. 5) assuming a single cavity located in a straight section, with peak voltage 19 kV. The agreement with theory

Table 1: First order and longitudinal motion tracking results.

E (MeV)	orbit length (m)	f_{rev} (MHz)	mom. compac.	synchr. tune
10	28.6333	1.5165	0.11605	0.01133
22	29.9794	2.1245	0.11611	0.00759
43	31.1885	2.8089	0.11616	0.00534
125	33.2724	4.2386	0.11619	0.00291

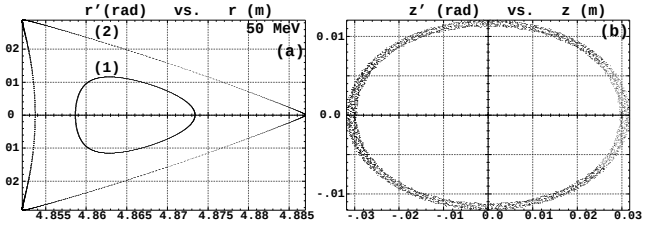

Figure 4: (a) : pure radial motion, particles launched with $r_0 = r_{c.o.} + 0.5$ cm (1) and at the stability limit (2). (b) : vertical motion, given $r_0 = r_{c.o.}$.

(*e.g.*, bucket height, synchrotron tunes - Tab. 1) is excellent over the all energy span of the FFAG.

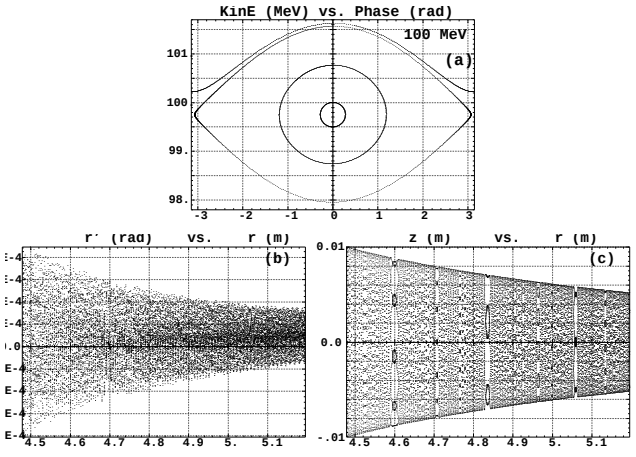

Figure 5: (a) : stationary bucket in the 100 MeV orbit region. (b, c) : respectively (r, r') and (r, z) motions during $12 \rightarrow 150$ MeV acceleration, for a particle launched near the 12 MeV horizontal closed orbit with $z_0 = 1$ cm ; the vertical damping follows $\sqrt{B\rho}$.

Eventually, a full acceleration cycle, $2\,10^4$ turns from 12 to 150 MeV, using 20 deg. synchronous phase, has been performed, sample results are given in Fig. 5.

Using field maps

Magnetic field maps can be used (Fig. 6-a), even in such highly non-linear problem. This is illustrated in Fig. 6-b which displays the horizontal motion stability limits and corresponding large amplitude tunes, at five different energies, as obtained by multiturn tracking, which clearly show good simplecticity behavior. There are two *sine qua non*

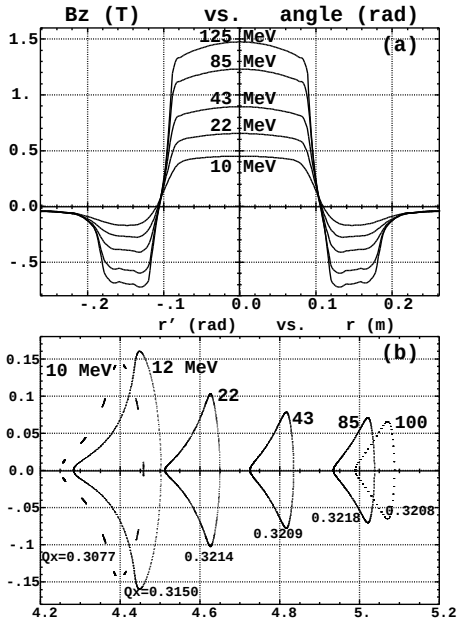

Figure 6: (a) : magnetic fi eld along closed orbits, drawn by tracking in TOSCA 3-D fi eld maps [13]. (b) : corresponding horizontal stable motion limits and large amplitude tunes.

Table 2: CPU time.

CPU time (seconds per turn per particle) :				
	Pentium III 1 GHz		Xeon 2.8 GHz	
	Analyt.	Num.	Analyt.	Num.
2nd order	0.17 s	0.40 s	0.10 s	0.25 s
4th order	0.44 s	1.00 s	0.17 s	0.64 s

conditions in getting precision, multiturn tracking. First, the integrator must be good, RK4 methods for instance would not allow simplectic tracking too far out of the median plane, by contrast with the Zgoubi method. Second, the map mesh must be dense, so as to insure a good interpolation of the - fast oscillating, see Fig. 2-d - derivatives which intervene in Eq. 1.

COMMENTS

Computation of field derivatives by numerical differentiation from the mid-plane geometrical field model (Fig. 2) yields good tracking symplecticity, in particular transverse motion (Fig. 4) can be explored up to stability limits. However, using analytical expressions instead for computing the derivatives insures best precision, and allows faster tracking, by a factor of more than 2.

Acceleration and 6-D motion are very well handled (Fig. 5). These developments yield an efficient ray-tracing tool for multi-particle, or long-term, tracking based studies, and, accounting for the built-in fitting procedure, for FFAG magnetic field and machine design studies.

CPU time - Computing speed tests were performed

upon $12 \rightarrow 150$ MeV acceleration in the 12 cell FFAG ring (conditions as in Fig. 5), using two different processors, Pentium III 1 GHz or Xeon 2.8 GHz, under Linux system. An integration step size $\Delta s = 0.5$ cm is considered, derivatives are computed with either the analytical or the numerical method, up to either second or fourth order as indicated in Tab.. 2. Such computing speed means that one can envisage overnight runs on computer network systems, aiming at such goals as long-term DA tracking, 6-D multi-turn beam transmission, resonance crossing studies.

ISOCHRONOUS LATTICE

A positive chromaticity, isochronous FFAG cell (Fig. 7-a), has been designed by G. Rees [8], for the purpose of fast (16-turn) acceleration of muons in the Neutrino Factory. Isochronism has been obtained by means of the non-linear

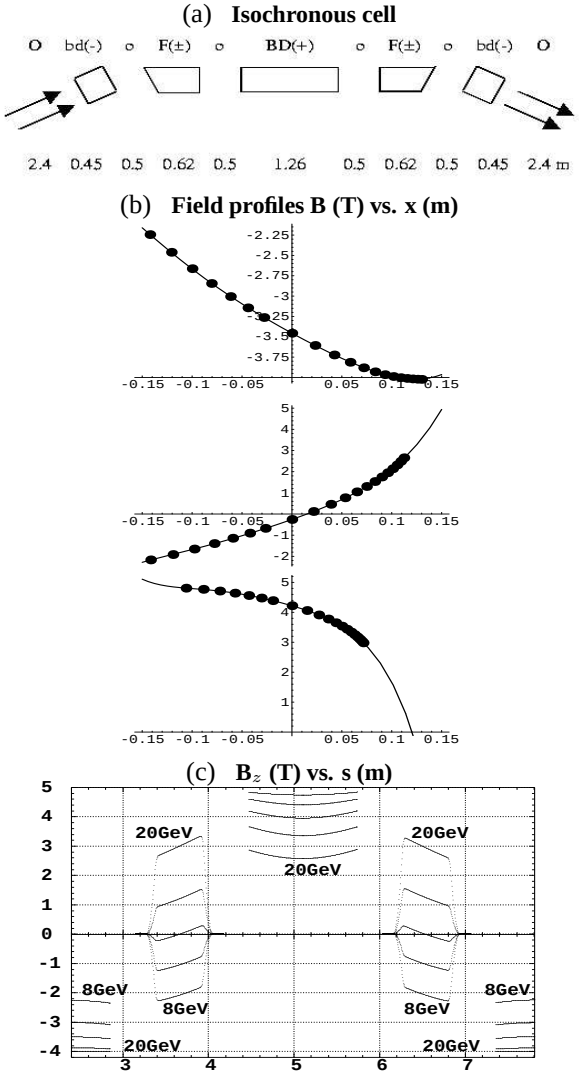

Figure 7: (a) isochronous cell, mirror-symmetric. (b) transverse profi le of magnetic fi elds in the three types of dipoles of the cell, bd, BF, BD (from top to bottom). (c) fi eld on closed orbits along the cell, at 8, 95, 11, 14 and 20 GeV.

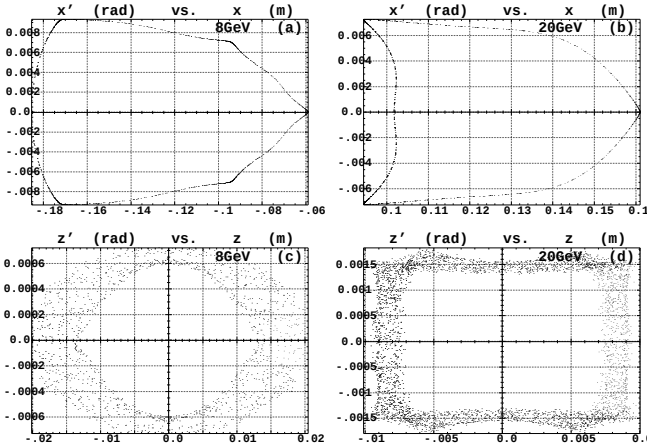

Figure 8: 1000-cell tracking, motion stability limits at better than 0.1 cm precision : (a,b) pure horizontal motion, (c,d) vertical motion at vicinity of horizontal closed orbit.

transverse field profiles schown in Fig. 7-b,c,d. Such field shapes can be reproduced for the ray-tracing purposes by using the mid-plane field model in Eq. 3, given adequate b_i coefficients obtained by matching, and yielding typical fields on closed orbits shown in Fig. 7-e.

A main interest of this particular type of "non-scaling" FFAG design, with cyclotron-like longitudinal behavior, is in its yielding best use of the high gradient, 200 MHz RF acceleration. It also allows use of insertions in the ring.

This type of lattice provides a good illustration of the power of stepwise ray-tracing : the design parameterization requires precision, in particular the isochronism has to be controlled at a the 10^{-6} level, which means necessary accuracy on the description of the strongly non-linear magnetic fields in the cell dipoles, and on ray-tracing. Typical outcomes of good symplecticity tracking are the motion stability limits - in other words, the cell acceptance, of prime interest - as displayed in Fig. 8.

ADJUSTED FIELD PROFILE LATTICE

This type of non-scaling FFAG lattice has recently been proposed by A.G. Ruggiero for application in GeV range proton machines [10, 14].

The longitudinally "Adjusted Field Profile" causes the index to be a function of the radial displacement x and of the longitudinal position, that is $n = n(x, \theta)$ (Fig. 9), so cancelling the momentum dependence of the focusing strength, a consequence being a reduced "non-scaling" : the variation of the total tune is only of the order of a fraction of an integer over the full acceleration cycle (Fig. 10). This method has been applied with dipole triplet cells that have been found to be advantageous, especially in the FDF configuration that yields low dispersion (Fig. 10). This type of design is believed to yield competitive technology that can allow beam performance at the level of the other accel-

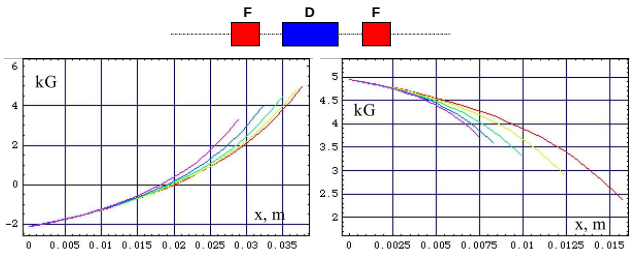

Figure 9: Field profiles vs. radial excursion at some azimuths in the F- (left graph) and D-sector (right) AFP magnets.

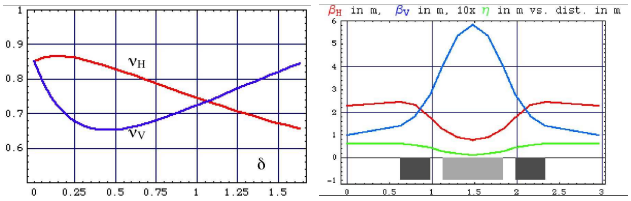

Figure 10: Left : total tunes only vary by a fraction of an integer during acceleration. Right : optical functions in the adjusted field profile non-scaling FDF cell.

erator architectures. A main feature is in the compactness of the magnets ensuing from the much reduced beam excursion, compared to scaling FFAG.

Developments in the ray-tracing code Zgoubi are now in progress, in order to allow simulation of these (x, θ)-dependent, non-linear, sector fields. The principle is in using the polynomial mid-plane modelling of Eq. 2 with radial dependence $\mathcal{R}_i$ as in Eq. 3, yet with the b_i coefficients functions of the azimuth θ in all three dipoles, namely

$$\mathcal{R}_{i=1-3}(x,\theta) = b_{0,i}(\theta) + b_{1,i}(\theta)\, x + b_{2,i}(\theta)\, x^2 + \ ...$$

Acknowledgements

I thank G. Rees and A. G. Ruggiero for their comments on the manuscript.

REFERENCES

[1] O CAMELOT ! A Memoir Of The MURA Years (Section 7.1), F.T.Cole, Proc. Cycl. Conf, April 11, 1994 ; FFAG particle accelerators, K.R. Symon et als., Phys.Rev. Vol.103-6, 1837-1859, 1956.

[2] (a) The ray-tracing code Zgoubi, F. Méot, NIM A 427 (1999) 353-356 ; (b) Zgoubi users' guide, F. Méot and S. Valero, CEA DAPNIA SEA-97-13/FERMILAB-TM-2010 (1997).

[3] Effect of the diagnostic undulator in IR4 on the LHC beam, F. Méot and A. Verdier, LHC-Note, 2004 ;
Concerning effects of fringe fields and longitudinal distribution of b_{10} in LHC low-β regions, F. Méot and A. París, Report FERMILAB-TM-2017, 1997 ;
On the effects of fringe fields in the LHC ring, F. Méot, Particle Accelerators, Vol. 52, 1996.

[4] Recycler ring studies, F. Méot, Report FERMILAB-TM-2016, Aug. 1997

[5] 50 GeV muon storage ring studies, C. Johnstone and F. Méot, Procs. PAC 2001 ;
On the effects of fringe fields in the CERN 50 GeV muon storage ring, F. Méot, CERN NuFact-Note-106 , 2000.

[6] Review of Current FFAG Lattice Studies in North Am., J.S. Berg et als., 17th Int. Conf. Cyclotrons (Tokyo, 2004).

[7] Developments in the ray-tracing code Zgoubi for multiturn tracking in FFAG rings, F. Lemuet, F. Méot, submitted for publication in NIM A.

[8] An isochronous ring for muon acceleration, G.H. Rees, FFAG04, KEK (2004).

[9] Normal and superconducting magnets for FFAG, T. Ogitsu, Procs. NuFact03 (N.Y., 2003).

[10] FFAG-Based High-Intensity Proton Drivers, A. G. Ruggiero, Invited Talk to the ICFA-HB2004 Workshop, October 18-22, 2004, Bensheim, Germany.

[11] Status of 150MeV FFAG synchrotron, S. Machida et als., Proc. PAC03 Conference.

[12] Determination of KEK 150 MeV FFAG parameters from ray-tracing in field maps, M. Aiba and F. Méot, CERN-NUFACT-Note-140 (2004).

[13] Field maps provided by M. Aiba, KEK, summer 2004.

[14] Adjusted Field Profile for the Chromaticity Cancellation in a FFAG Accelerator, A. G. Ruggiero, Contribution to ICFA-HB2004, October 18-22, 2004, Bensheim, Germany.